THE ASTRONOMICAL JOURNAL VOLUME 107, NUMBER 6 JUNE 1994

SEARCHING FOR CLUSTER MAGNETIC FIELDS IN THE COOLING FLOWS OF 0745−191, A2029, AND A4059

GREGORY B. TAYLOR AND ELIZABETH J. BARTON
Radio Astronomy 105-24, California Institute of Technology, Pasadena, California 91125
Electronic mail: gbt@astro.caltech.edu

JINGPING GE
Physics Department, Brandeis University, Boston, Massachusetts 02254
Electronic mail: jpg@vlbi.astro.brandeis.edu

Received 1993 November 29; revised 1994 January 26

ABSTRACT

We have performed sensitive polarimetric radio observations with the VLA of three galaxies: PKS 0745−191, PKS 1508+059, and PKS 2354−350, embedded in x-ray cooling flow clusters. High sensitivity, multifrequency maps of all three, along with spectral index and Faraday rotation measure (RM) maps of PKS 1508+059 and PKS 2354−350 are presented. For PKS 1508+059 and PKS 2354−350 models of the electron density of the intracluster medium (ICM) have been used to set lower limits of 0.1 and 2.7 μG, respectively, on the magnetic field in the ICM based on the observed RMs. In an x-ray selected sample of cooling flow clusters with an associated radio source, 57% (8/14) are found to have absolute RMs in excess of 800 radians m^{-2}. This sample includes the three sources of this study and *all* the other high RM sources found to date at $z<0.4$. These facts are consistent with the high RM phenomenon being produced by magnetic fields associated with the relatively dense, hot x-ray gas in cooling flow clusters.

1. INTRODUCTION

Radio sources embedded within rich clusters of galaxies can serve as useful probes of the intracluster medium (ICM). Sharp changes in the ICM pressure at the sonic radius may disrupt radio jets (Soker & Sarazin 1988; Norman *et al.* 1988), and if the thermal ICM pressure is large enough it may confine the radio source. Polarized radiation from embedded radio sources may also be rotated by the Faraday effect if magnetic fields are present in the ICM.

The x-ray emission in some clusters is strongly peaked at the center, leading to high densities and cooling times of the hot ICM in the inner ~100 kpc of much less than the Hubble time. To maintain hydrostatic equilibrium, an inward flow is required (for a review see Fabian *et al.* 1991). Typical mass cooling flow rates are 100 $M_\odot$ yr^{-1}. No direct evidence has yet emerged, however, either for the "flow" of material into the center, or for where the "cooled" gas resides. Nevertheless, as is done in the literature, we will use the terminology "cooling flow" to refer to this observational class of sources. The cooling flow phenomenon in clusters is quite common—between 70%–90% of an x-ray flux-limited sample of clusters have cooling flows (Edge *et al.* 1992).

While most extragalactic radio sources exhibit Faraday rotation measures (RMs) on the order of 10 s of radians m^{-2} due to the interstellar medium of our galaxy, there are a small number of sources displaying RMs in excess of ~1000 radians m^{-2}. Recent studies of these high RM sources [e.g., Cygnus A: Dreher, *et al.* (1987); A1795: Ge & Owen (1993); Hydra A: Taylor & Perley (1993)] indicate that these RMs are most likely to be induced by a cluster magnetic field. Furthermore a common theme has emerged that each of the high RM sources is found in association with a hot x-ray emitting gas, and in most cases a cooling flow (Ge 1991; Taylor 1991). The diversity of the radio structures and powers, and the commonality of the x-ray parameters suggest that the high RMs are the result of external Faraday rotation occurring in a magnetized hot cluster gas surrounding the radio sources. For external Faraday rotation, the RMs are related to the density, n_e, and magnetic field along the line of sight, $B_\parallel$, through the cluster according to

$$\mathrm{RM}=812\int_0^L n_e B_\parallel \, dl \text{ radians m}^{-2}, \quad (1)$$

where $B_\parallel$ is measured in μGauss, n_e in cm^{-3} and dl in kpc. the RM distribution, along with x-ray observations (used to estimate n_e), can then be used to understand the magnetic field structure along the line of sight.

The RM structure of many of the high RM sources (in particular that of Hydra A, 3C 295, Cygnus A, and A1795) show ordered structures over tens to hundreds of kpc. The origin and evolution of such magnetic fields is a topic of some speculation (Daly & Loeb 1990; Goldman & Rephaeli 1991; DeYoung 1992). They could be remnant magnetic fields of extinct radio galaxies, the result of a cluster dynamo effect (Ruzmaikan *et al.* 1989; Eilek 1993), or magnetic fields stripped from spiral galaxies during galactic cannibalism. Cluster magnetic fields may have important effects on cluster dynamics and energy transport (Sarazin 1986; Tribble 1989), and significant implications for primordial star formation (Pudritz & Silk 1989). These magnetic fields can only be traced when there is a radio source located within or behind the cluster. Given the low density of sources fortuitously

 0004-6256/94/107(6)/1942/11/$0.90

located behind clusters and strong enough to provide a good estimate of the RM, the best way to probe these fields is to examine those clusters with a known radio source.

We have observed PKS 0745−191, PKS 1508+059, and PKS 2354−350 in order to test the predictions of Ge (1991) and Taylor (1991) that radio galaxies in cooling flow clusters exhibit high RMs. We also use the detailed observations of these sources in an attempt to better understand their environment. We present our observations in Sec. 3. In Sec. 4 we compare thermal and radio pressures, derive spectral indices, and present the RM results. In Sec. 5 we discuss the RM observations for a sample of radio sources embedded in cooling flows. We assume $H_0=50$ km s^{-1} Mpc^{-1} and $\Omega=1$ throughout this paper.

2. PREVIOUS OBSERVATIONS

All three radio sources lie in rich, Bautz-Morgan (1970) type I clusters; PKS 0745−191 in 0745−191, PKS 1508+059 in A2029, and PKS 2354−350 in A4059. Furthermore, each radio source is associated with an ultraluminous cD galaxy (0745−191—Mackie *et al.* 1990; A2029—Uson *et al.* 1991; A4059—Carter *et al.* 1985). Each of these clusters is a luminous x-ray source, and in fact 0745−191 is the most luminous x-ray cluster found in a flux limited sample of 51 sources (Edge *et al.* 1992). All three sources possess significant cooling flows.

PKS 0745−191 has been imaged extensively in the radio by Baum & O'Dea (1991), and was included, along with PKS 1508+059, in a study of the radio properties of cD galaxies in clusters by Burns (1990). Sumi *et al.* (1988) presented high resolution VLA images of PKS 1508+059 at 4860 and 1500 MHz. We have retrieved this data, along with unpublished observations from the VLA archive, in order to produce high resolution, multifrequency spectral index and polarization maps. The only previous radio image of PKS 2354−350 comes from Ekers *et al.* (1989) using the partially completed VLA.

3. THE VLA OBSERVATIONS

These sources were selected for sensitive, high resolution polarimetry by their large cluster cooling flow rates, the presence of extended radio emission, and the fact that no previous RM determination existed. Observations of PKS 0745−191, PKS 1508+059 and PKS 2354−350 were made with the Very Large Array (VLA) of the NRAO[1] at four frequencies within the 3.6 cm band in order to map the RM structure. For both PKS 1508+059 and PKS 2354−350 observations were made in both the A and A/B or B configurations, and later combined, in order to provide both high spatial resolution and good sensitivity to diffuse polarized emission on scales of 5″–10″. Supplemental observations were also made at 4860 MHz, or obtained from the VLA archive in the case of PKS 1508+059. Table 1 contains a list of the observations.

TABLE 1. VLA observations.

Source	Date	Configuration	Frequencies (MHz)	Duration (hrs)	Bandwidth (MHz)
PKS0745-191	1992 Nov 14	A	7815, 8165	1.99	50
			8515, 8885	1.97	50
PKS1508+059	1985 May 16	B	4835, 4885	5.39	50
	1985 Jul 14	C	4835, 4885	4.05	50
	1986 Jun 21	A/B	1465, 1515	0.71	50
			4835, 4885	2.87	50
	1987 Sep 6	A	1465, 1515	1.01	50
	1987 Dec 19	B	14915, 14965	3.74	50
	1988 Mar 16	C	14915, 14965	1.08	50
	1992 Nov 14	A	7815, 8165	2.04	50
			8515, 8885	1.98	50
	1993 Mar 24	B	7815, 8165	1.20	50
			8515, 8885	1.20	50
PKS2354-350	1992 Nov 14	A	7815, 8165	2.27	50
			8515, 8885	2.24	50
	1993 Feb 7	B	4815, 4885	0.41	50
			7815, 8165	0.89	50
			8515, 8885	0.89	50

Absolute flux calibration to the flux scale of Baars *et al.* (1977) was obtained through a short observation of 3C 286. Complex antenna gain and polarization calibration were performed using nearby VLA calibrators in the standard way. All calibration and mapping were performed using the AIPS package of the NRAO.

4. RESULTS

4.1 Multifrequency Synthesis Radio Images

Byproducts of the multifrequency observations required for the RM determinations are four sensitive total intensity

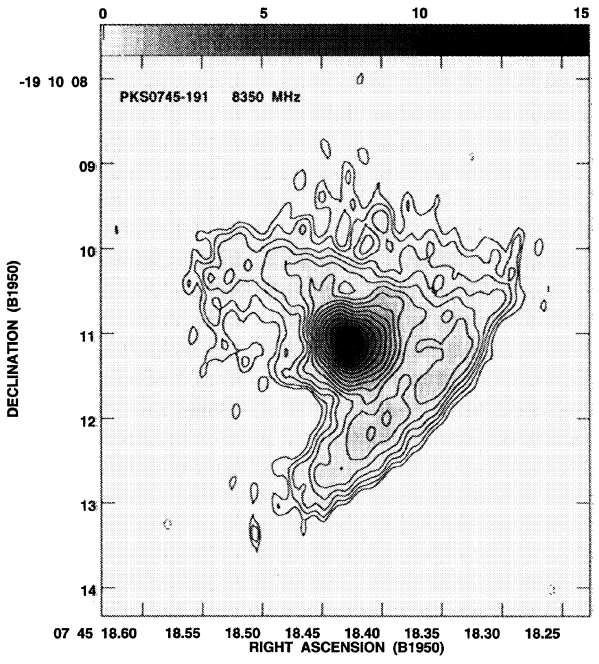

FIG. 1. The 8350 MHz (3.6 cm) image of PKS 0745−191 made by multifrequency synthesis. The synthesized beam is 0.264″×0.170″ at p. a. −6°. Contours are drawn at −0.1, 0.1, 0.141, 0.2, ..., 25.6 mJy beam^{-1} at root two intervals with negative contours drawn using dashed lines. The greyscale range is from 0 to 15 mJy beam^{-1}.

[1]The National Radio Astronomy Observatory is operated by Associated Universities, Inc., under cooperative agreement with the National Science Foundation

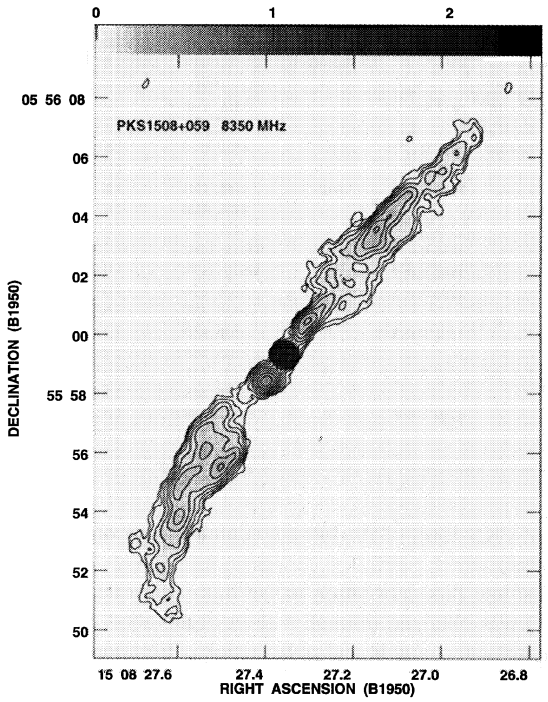

FIG. 2. The 8350 MHz image of PKS 1508+059 made by multifrequency synthesis and combined observations from the A and B configurations of the VLA. The synthesized beam is 0.4″. Contours are drawn at −0.04, 0.04, 0.057, 0.08, ..., 2.56 mJy beam^{-1} at root two intervals with negative contours drawn using dashed lines. The greyscale range is from 0 to 2.5 mJy beam^{-1}.

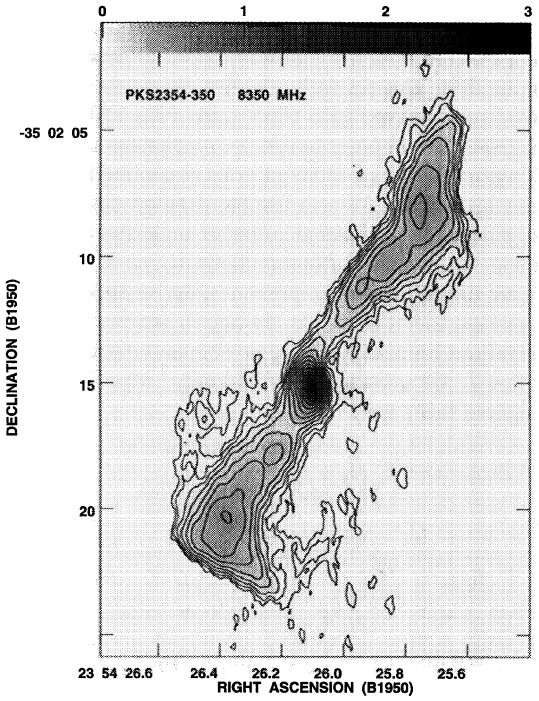

FIG. 3. The 8350 MHz image of PKS 2354−350 made by multifrequency synthesis and combined observations from the A and A/B configurations of the VLA. The synthesized beam is 0.8″×0.5″ at p.a. 7°. Contours are drawn at −0.05, 0.05, 0.071, 0.1, ..., 3.2 mJy beam^{-1} at root two intervals with negative contours drawn using dashed lines. The greyscale range is from 0 to 3 mJy beam^{-1}.

measurements with a frequency spread of 14%. This frequency spread is nearly ideal for covering gaps in the $u-v$ plane and can make a considerable improvement in both sensitivity and image fidelity (Conway 1991). Differences in the spectral index between the strong core and diffuse emission in PKS 0745−191 led to weak but significant spectral sidelobes. To eliminate these sidelobes the core component was removed, the four frequencies combined, and then the core component added back to the $u-v$ data. The uniformly weighted image made from this synthesis is shown in Fig. 1.

Total intensity images of PKS 1508+059 and PKS 2354−350 made directly from a multifrequency synthesis and using natural weighting are shown in Figs. 2 and 3. The positions of the radio core, accurate to ±50 mas, are presented for each image in Table 2 along with the redshift, 1400 MHz power and largest angular size (LAS). The beam, rms noise, peak core flux density, and total source flux density for each of these images is given in Table 3, along with measurements from observations at other wavelengths. The errors in the peak and total flux densities are typically ~2%. The measurements of total flux density generally agree with previous single dish measurements, although we find only 76 mJy for PKS 2354−350 at 4860 MHz compared to 110 mJy found by Ekers *et al.* (1989) using the Parkes 64 m telescope. The missing flux is the result of insufficient short baselines.

4.2 Spectral Indices

The integrated radio spectrum for each source (Fig. 4) was derived using published values from the literature and our own observations. At low frequencies these data come primarily from single dish observations (taken from the Parkes 1990 Catalog of the Australia Telescope National Fa-

TABLE 2. Radio parameters.

Source	Core Position (B1950)[a]		z	log P_{1400}	scale	LAS[b]
	R.A.	Decl.		(W Hz^{-1})	(kpc asec^{-1})	(kpc)
PKS0745−191	07 45 18.427	−19 10 11.13	0.1028	25.99	2.52	25
PKS1508+059	15 08 27.357	05 55 59.30	0.0767	25.13	1.96	80
PKS2354−350	23 54 26.103	−35 02 15.12	0.0478	25.11	1.28	70

[a] Core positions were determined from the 8350 MHz images.
[b] The largest angular size (LAS) was determined from the 4860 MHz images.

TABLE 3. Radio flux density measurements.

Source	Freq. (MHz)	Beam (asec)	rms (mJy beam^{-1})	Peak (mJy beam^{-1})	Total Flux (mJy)
PKS0745−191	8350	0.264 × 0.170 at −5.7°	0.031	34.8	168
PKS1508+059	1490	1.3 × 1.3	0.078	29.9	511
	4860	1.3 × 1.3	0.026	5.1	58.5
	8350	0.4 × 0.4	0.010	2.9	25.0
	14940	0.72 × 0.62 at −61°	0.048	2.2	9.7
PKS2354−350	8350	0.8 × 0.5 at 7°	0.011	3.0	37.0
	4860	1.67 × 1.22 at 20°	0.047	7.5	75.6

cility, and from the Effelsberg survey of Andernach *et al.* 1988). At high frequencies the data are primarily derived from VLA observations (Owen *et al.* 1992; Ekers *et al.* 1989; Baum & O'Dea 1991; this work). For PKS 2354−350 at 5000 MHz we have used the value reported by Ekers *et al.* (1989). A linear least-squares fit to the data yield spectral indices, α, (defined as $S_\nu \propto \nu^\alpha$) of −1.22, −1.52, and −1.43 for PKS 0745−191, PKS 1508+059, and PKS 2354−350 respectively. These spectral indices are much steeper than the median α of ~−0.68 (Windhorst *et al.* 1990) for sources with comparable radio powers, but are similar to other sources in dense cooling flow clusters (e.g., 3C 295—Perley & Taylor 1991; Hydra A—Taylor *et al.* 1990).

Spectral index maps for PKS 0745−191 can be found in Baum & O'Dea (1991).

In Fig. 5(a) we show a spectral index map of PKS 1508 +059 between 4860 and 8515 MHz. The spectral index is 0.21 at the core and steepens to −2.7 near the edges of the source. In Fig. 5(b) is the spectral index map between 1490 and 4860 MHz. This map reveals faint tails with a steep spectrum of ~−3. Evidence for curvature in the spectrum of PKS 1508+059 can be found by comparing Figs. 5(a) and 5(b). The spectral index of the jet is steeper in the spectral index map made with the higher frequency pair.

The spectral index map for PKS 2354−350 between 4860 and 8515 MHz is shown in Fig. 6. The spectral index is −1 at the core and steepens slightly to −1.1 in the lobes. There is some evidence for a faint, diffuse component to the lobes with a spectral index of −2.5 or perhaps even steeper. This is supported by the missing flux in the 4860 MHz synthesis image compared to the single dish measurement (see Sec. *4.1*). Some of this faint, diffuse emission can be seen in a 4860 MHz image made using a larger, 5″ beam (Fig. 7). Accurate measurements of the flux density and spectral index of this diffuse component will require further observations which include shorter spacings.

Since high energy electrons radiate faster than those at lower energies, the age of a synchrotron source can be related to its spectral shape (Scheuer & Williams 1968; Myers & Spangler 1985). Assuming an injected power law spectrum corresponding to a spectral index of −1 and synchrotron losses in which electrons retain constant pitch angles, we have used the derivation of Myers and Spangler to estimate the age of the source. In the jets of PKS 1508+059, the minimum energy magnetic field strength is ~50 μG, and the spectral index is ~−1.5, leading to an estimated age for the jets of 1.1×10^6 yr. In the tails the spectral index steepens to ~−2.5 and the minimum energy field strength falls to ~20 μG which gives an age of 12×10^6 yr. This age requires an average bulk velocity of 3200 km s^{-1} if the relativistic electrons that supply the tail come from the central engine within the radio core.

4.3 Comparison of X-ray and Radio Pressures

We have calculated the minimum energy magnetic field strengths and pressures in several locations in each source. This has been done assuming a cylindrical geometry as in Perley *et al.* (1979). We have further assumed a volume filling factor, η, of unity, upper and lower frequency cutoffs of

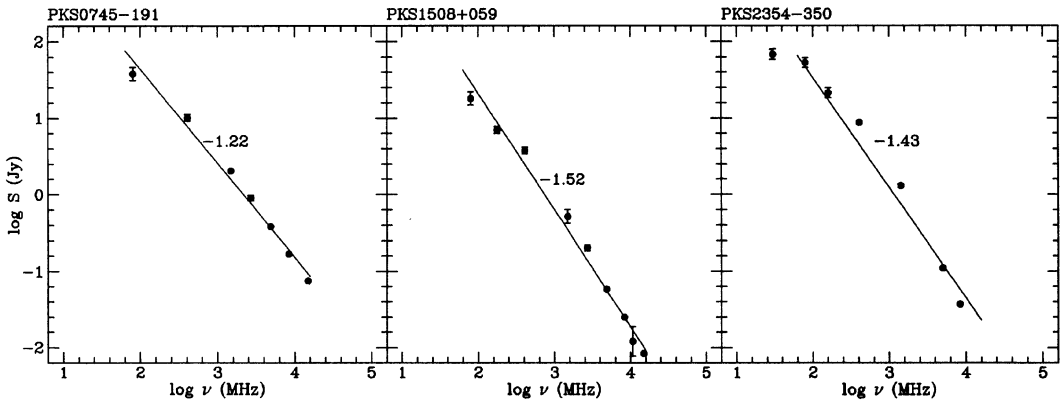

FIG. 4. The integrated spectra for PKS 0745−191, PKS 1508+059, and PKS 2354−350. Total flux density measurements were taken from the literature (see text for references) as well as the observations presented in this paper. A single power law has been fit to each data set and its corresponding index is shown.

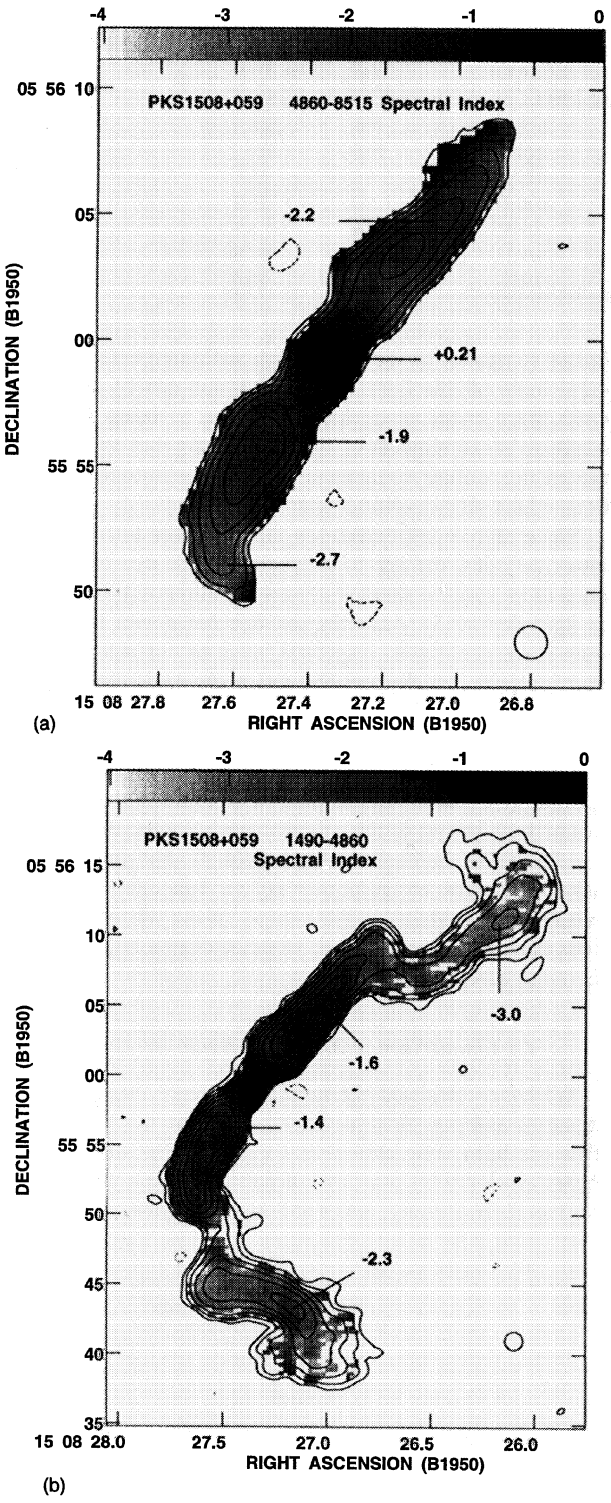

FIG. 5. Spectral index maps of PKS 1508+059 at 1.3″ resolution made between 4860 and 8515 MHz overlaid on contours from an 8515 MHz image (a) and between 1490 and 4860 MHz overlaid on contours from the 1490 MHz image (b). The greyscale range is from 0 to −4 for both maps. The FWHM of the synthesized beam is drawn in the lower right corner. Contours increase by factors of 2 with the lowest contour starting at 0.06 and 0.24 mJy beam^{-1} in (a) and (b), respectively.

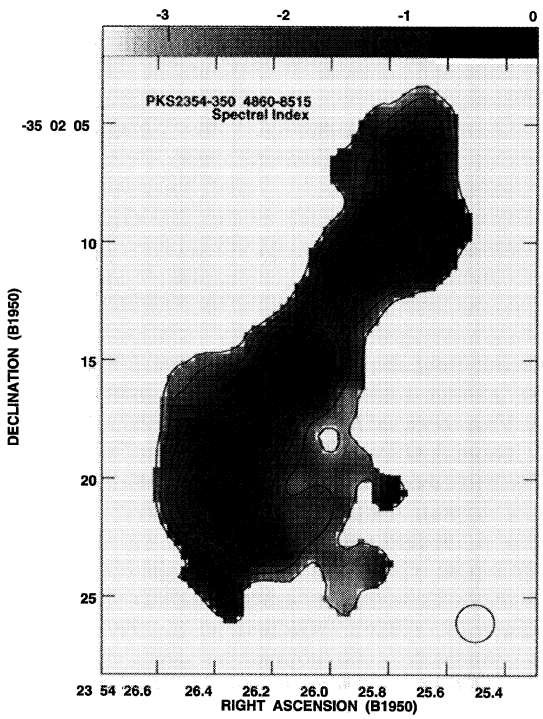

FIG. 6. Spectral index map of PKS 2354−350 at 1.6″ resolution made between 4860 and 8515 MHz. The greyscale range is from 0 to −3.5. Contours are taken from the 8515 MHz image and drawn at 0.08, 0.16, 0.32, 0.64, 1.3, 2.6, and 5.1 mJy beam^{-1}.

10 GHz and 10 MHz, and equal energies in the relativistic electrons and protons. The spectral index used for the calculations is taken from the measured value between 1490 and 4860 MHz. The values are presented in Table 4, along with the thermal pressure derived from x-ray observations.

In PKS 0745−191 and PKS 1508−059 the thermal pressures derived from the x-ray observations exceed the minimum energy pressures derived from the radio observations by up to two orders of magnitude. In PKS 2354−350 the x-ray observations of Schwartz *et al.* (1991) provide only a lower limit to the central density and thermal pressures, which are probably much greater. All three radio sources may be confined by the hot gas, in which case their energies must be somewhat greater than the minimum energy conditions. Alternatively, the radio sources might be filamentary with volume filling factors less than unity since $P_{me} \propto \eta^{-4/7}$. To be unconfined by the large thermal pressures would require the radio sources to be highly filamentary, and/or to have energies over two orders of magnitude greater than the minimum energy. Confinement of the radio sources is consistent with their relatively small sizes and steep spectra.

4.4 Comparison of X-ray and Radio Images

In Fig. 8 the 20 cm radio image of PKS 1508+059 is overlaid on the *ROSAT* HRI image (Sarazin *et al.* 1992; hereafter referred to as SOM). The *ROSAT* image has been shifted by 0.5″ and 3.3″ in right ascension and declination, respectively, in order to align the x-ray peak with the radio

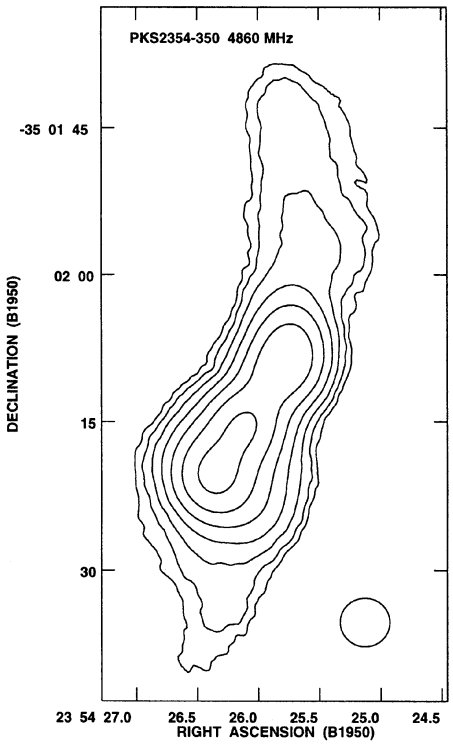

FIG. 7. An image of PKS 2354−350 at 4860 MHz and 5″ resolution. Note the presence of faint, diffuse emission to the north and south. Contours are drawn at 0.2, 0.4, 0.8, 1.6, 3.2, 6.4, and 12.8 mJy beam^{-1}.

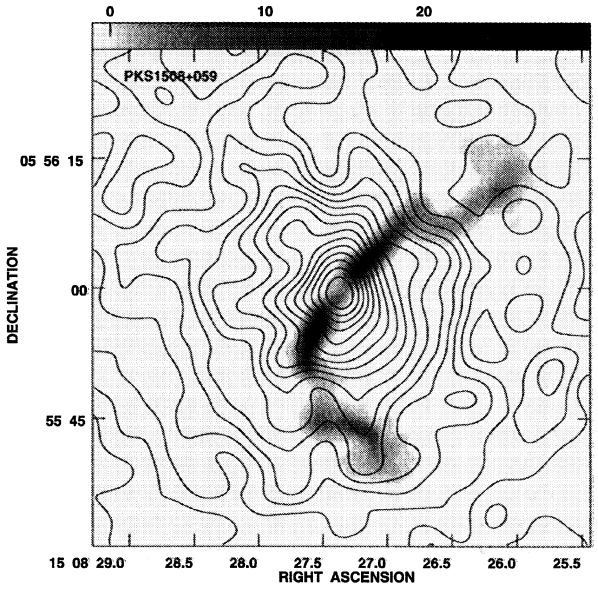

FIG. 8. The 1490 MHz radio image at 1.3″ resolution overlaid upon the *ROSAT* HRI image at 2″ resolution from Sarazin *et al.* (1992). The x-ray image has been shifted such that the peak of the x-ray emission is coincident with the radio core. Contours are drawn at 5%, 10%, 15%, ..., 95% of the peak x-ray flux. The greyscale range is from −1 to 30 mJy beam^{-1}.

core. This shift is marginally consistent with the error in the position of the x-ray centroid of ±3″ quoted by SOM. With the two images aligned, it is evident in Fig. 8 that the radio emission is anticoincident with the x-ray filaments. In other words, the radio emission appears to flow out along a pressure minimum, as expected for a buoyantly rising plume. A similar, but more pronounced, effect has recently been reported for NGC 1275 (3C84) by Böhringer *et al.* (1993). The idea of a radio-emitting plasma buoyantly rising through a hot gas goes back to the work of Gull & Northover (1973). The velocity for a buoyantly rising plasma in a constant pressure gradient is

$$v = c_s \left(\frac{2\Delta\rho_{\rm ext}}{\rho_{\rm int}} \right)^{1/2}, \qquad (2)$$

where c_s is the speed of sound in the external medium, $\Delta\rho_{\rm ext}$ is the change in density in the external medium, and $\rho_{\rm int}$ is the density of the radio plasma. The sound speed in PKS 1508+059 is 1070 km s^{-1} which requires an internal density of 0.05 cm^{-3} in order to be consistent with the flow velocity of 2700 km s^{-1} derived from the change in spectral index (see Sec. *4.2*). Baum & O'Dea (1991) also suggest that the amorphous structure of PKS 0745−191 may be due to buoyancy effects, and find spectral indices consistent with a buoyant flow.

4.5 Rotation Measure Structure

Faraday rotation measures can be produced within an extragalactic radio source if sufficient thermal material is

TABLE 4. Minimum energy magnetic fields and pressures.

Source	Location	dist (asec)	B_{me} (μG)	P_{me} (dynes cm^{-2})	P^a_{th} (dynes cm^{-2})	n^a_{th} (cm^{-3})
PKS0745−191	SE Ridge	1.1	88	3.1×10^{-10}	8.0×10^{-10}	0.03
	NW Exten.	1.6	59	1.4×10^{-10}	8.0×10^{-10}	0.03
PKS1508+059	N Jet	4.4	50	1.0×10^{-10}	2.8×10^{-8}	1.25
	S Jet	4.6	49	9.7×10^{-11}	1.8×10^{-8}	0.80
	N Tail	20.8	20	1.6×10^{-11}	9.5×10^{-9}	0.42
	S Tail	15.1	23	2.2×10^{-11}	1.3×10^{-8}	0.58
PKS2354−350	N Lobe	8.5	28	3.1×10^{-11}	$>4.8 \times 10^{-11}$	>0.01
	S Lobe	6.8	37	5.6×10^{-11}	$>4.8 \times 10^{-11}$	>0.01

[a] X-ray pressures and densities are from Arnaud *et al.* 1987 for PKS0745−191; Sarazin, O'Connell & McNamara 1992 for PKS1508+059; and Schwartz *et al.* 1991 for PKS2354-151.

mixed in with the synchrotron radiating relativistic plasma (internal Faraday rotation), or along the line of sight by magnetic fields and thermal gas (external Faraday rotation). Recent studies (Ge 1991; Taylor 1991) of the high RM sources suggest that in all cases the dominant mechanism is external Faraday rotation. In the following three sections, the results of the multifrequency polarimetry are presented for each of the sources.

PKS 0745−191: No polarized flux was detected in PKS 0745−191 down to a 3σ limit of 45 μJy beam^{-1} at 8515 MHz. This is a factor of 3 lower than the limit obtained by Baum & O'Dea (1991) at 4860 MHz. Our corresponding limit on the core fractional polarization is <0.1%.

The very low polarization observed in PKS 0745−191 may be the result of: (1) a highly tangled magnetic field within the source; (2) depolarization by dense thermal gas intermixed with the radio-emitting plasma; or (3) depolarization by an external Faraday screen. The first possibility is highly unlikely since any shear or compression will strongly polarize the radio source (Laing 1980). Given the presence of the dense ICM and the large equipartition radio pressure, shear and compression are likely to occur. The second reason is also unlikely since PKS 0745−191 appears to be buoyantly flowing away from the cluster center. In addition, no convincing evidence for internal Faraday rotation has yet been found for any extragalactic radio source (Taylor & Perley 1993, 1994). All of the high RM sources are severely depolarized by an external Faraday screen when observed with low resolution and/or at low frequencies. We believe this mechanism is responsible for the low polarization observed from PKS 0745−191.

The depolarizing Faraday screen may be located in either the ICM or the line-emitting gas. If PKS 0745−191 is similar to the other high RM sources then the RM gradients in the ICM must exceed 2700 radians m^{-2} arcsec^{-1} everywhere across the source. Alternatively, PKS 0745−191 may be depolarized by magnetic fields associated with the line-emitting gas. Heckman *et al.* (1989) report on a strong emission-line region in PKS 0745−191 that completely covers the radio-emitting region. Furthermore, the volume filling factor is believed to be very small, 3.1×10^{-6} (Heckman *et al.* 1989), so that many filaments would exist within any telescope beam. If magnetized, these filaments would give rise to a wide range of RMs within each telescope beam and thereby depolarize the source. To provide sufficient coverage of filaments across the beam may require an ICM component associated with the line-emitting component, but with a larger filling factor. Depolarization at the location of line-emitting gas has also been seen in A1795 (Ge & Owen 1993).

PKS1508+059 in A2029: Most of the southeast lobe and the brighter part of the northern lobe in PKS 1508+059 were found to be as much as 50% polarized and had polarized flux densities of 50–120 μJy beam^{-1} in the 8 GHz band at 0.4″ resolution. The 4860 MHz data have been almost completely depolarized, probably due to large gradients in the RM (see below). The rms noise in the 8 GHz Stokes Q and U images was 14 μJy beam^{-1}. The RM image (Fig. 9) was determined from the 7815, 8165, 8515, and 8885 MHz 0.4″ resolution maps by performing a weighted linear least-squares fit on a pixel-by-pixel basis to the polarization angle, ψ, against λ^2. No value for the RM was determined unless the errors in ψ were less than 20°.

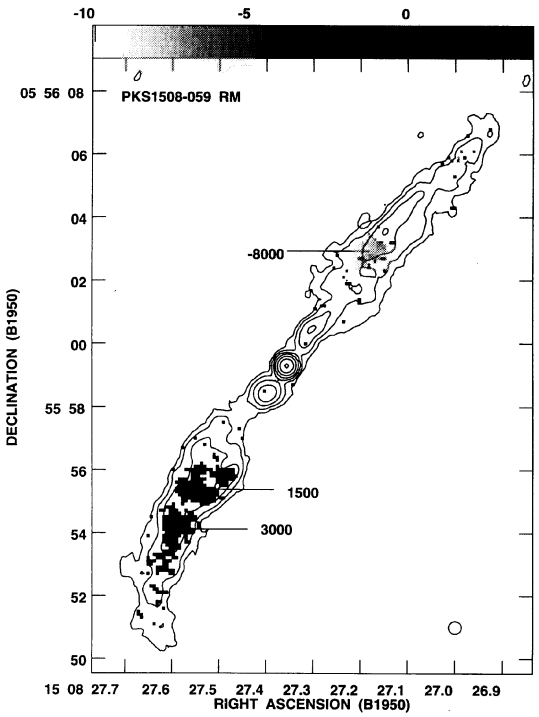

FIG. 9. The RM map in greyscale for PKS 1508+059 at 0.4″ resolution. The greyscale range is from −10 000 to 4000 radians m^{-2}. Contours are taken from the 8350 MHz image and drawn at 0.04, 0.08, 0.16, 0.32, 0.64, 1.3, and 2.6 mJy beam^{-1}.

In the southeast lobe the RMs start out around 200 radians m^{-2} in the region closest to the core and steadily increase with distance to a maximum value of 4000±400 radians m^{-2} at a distance of 5.6″ (11 kpc). The gradient in RM is ~2000 radians m^{-2} arcsec^{-1}. Even further out along the lobe the RMs appear to decrease, although the signal-to-noise ratio is low. In the northwest lobe the RMs are ~−8000±500 radians m^{-2}. Some sample fits of the RM are plotted in Fig. 10 at every other pixel for the northwest region. In all cases the data are well fit by a λ^2 relation. Using a power-law density distribution derived from the azimuthally averaged x-ray image (SOM 1992) out to a distance of 200 kpc, we derive a minimum cluster magnetic field strength of >0.19 μG to the northwest lobe. If the field is tangled, or confined to a smaller volume of the cluster, then its strength must be greater. Towards the southeast lobe, where the RMs are smaller we find a minimum cluster magnetic field strength of >0.11 μG. The change in sign of the RM from the northwest to southeast lobe indicates that a field reversal must take place. Field reversals across the core have been seen in two other high RM sources (A1795—Ge & Owen 1993; and Hydra A—Taylor & Perley 1993). The presence of these field reversals implies ordered cluster magnetic fields on scales of 20–100 kpc.

The projected magnetic field direction in the radio source, corrected for RM, is shown in Fig. 11. While some of the

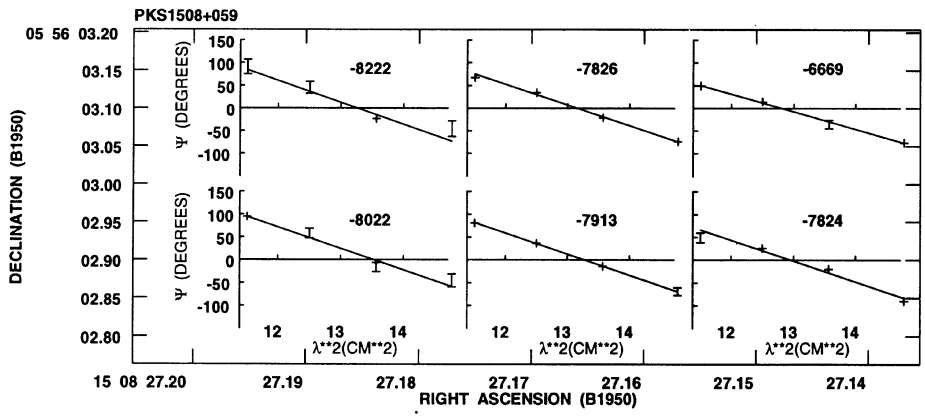

FIG. 10. Sample fits to the RM in the northwest lobe of PKS 1508+059. Error bars are drawn only if they would exceed the size of the plotted points. The separation between pixels is 0.2″, or half the beamwidth.

irregularity in the field orientation from pixel to pixel may be intrinsic to the source, much of it is probably due to errors in the RM determination. An error in the RM of ±300 radians m^{-2} will result in a rotation of ±21° at 8500 MHz.

PKS 2354−350 in A4059: At 8500 MHz PKS 2354−350 is more strongly polarized than PKS 1508−059. Polarized intensities range from 60–190 μJy $beam^{-1}$ and the fractional polarization in typically 40% and is as high as 80% in the lobes. There is one location in the southeast lobe where we find only an upper limit to the polarization of 7%. At 4860 MHz PKS 2354−350 is considerably less polarized than at 8500 MHz, reaching a maximum value of only 22%. A map of the depolarization (m_{8500}/m_{4860}) is shown in Fig. 12. Values for the depolarization range from 1.5–6. A depolarization of 2 could be caused by a gradient in the RM of 350 radians m^{-2} $arcsec^{-1}$.

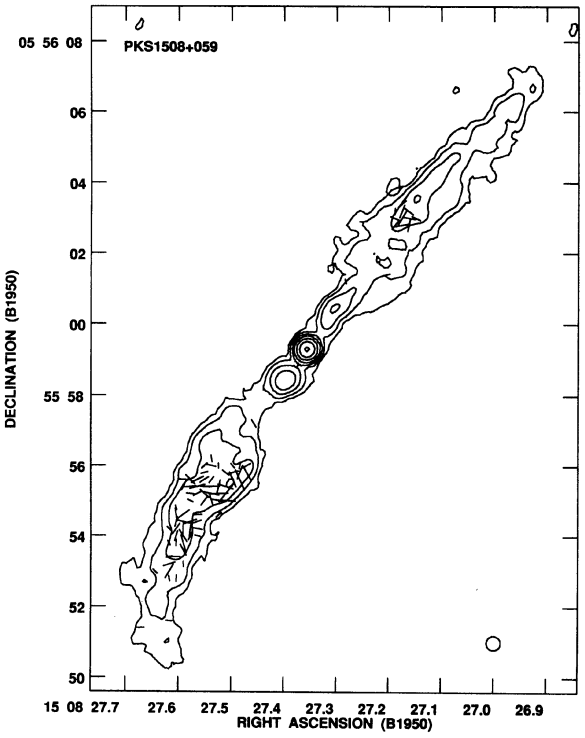

FIG. 11. The projected magnetic field direction, corrected for RM, in PKS 1508+059. A vector length of 1″ corresponds to a polarized intensity of 0.2 mJy $beam^{-1}$. Contours are taken from the 8350 MHz total intensity image and are the same as in Fig. 9.

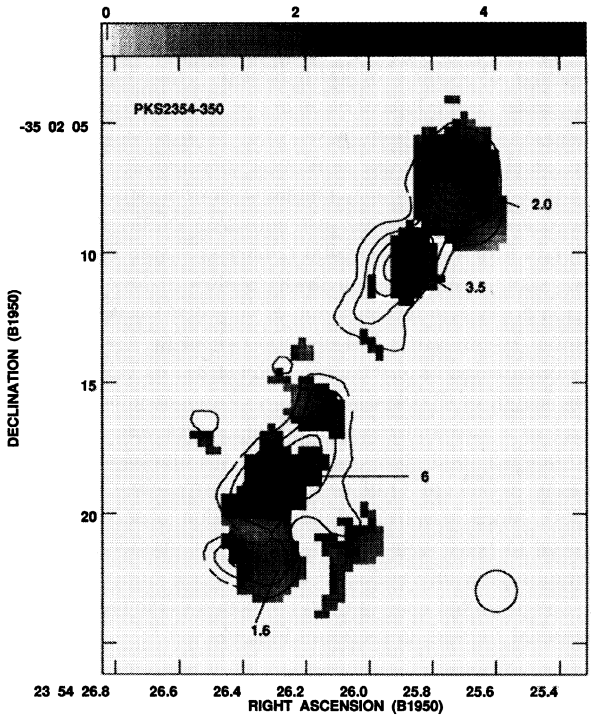

FIG. 12. The depolarization, (m_{8515}/m_{4860}), map for PKS 2354−350 at 1.6″ resolution. The contours are taken from the 8515 MHz polarized intensity image. Note that several regions for which there are no data (due to a lack of information at 4860 Mhz) are bordered by regions of very large depolarization. Contours are drawn at 0.05, 0.1, 0.2, 0.3, 0.4, 0.5, and 0.6 mJy $beam^{-1}$

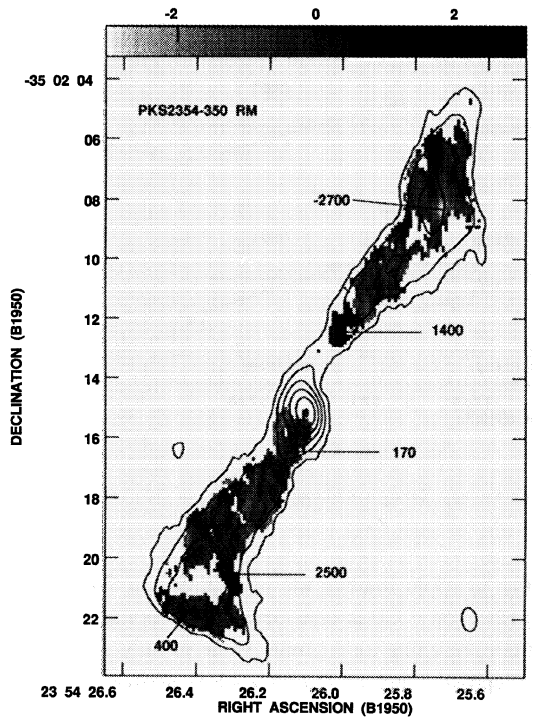

FIG. 13. The RM map in greyscale for PKS 2354−350 at 0.8″×0.5″ resolution. The greyscale range is from −3000 to +3000 radians m^{-2}. Contours are taken from the 8350 MHz image and drawn at 0.09, 0.18, 0.36, 0.72, 1.4, 2.9, and 5.8 mJy $beam^{-1}$. The separation between pixels is 0.4″.

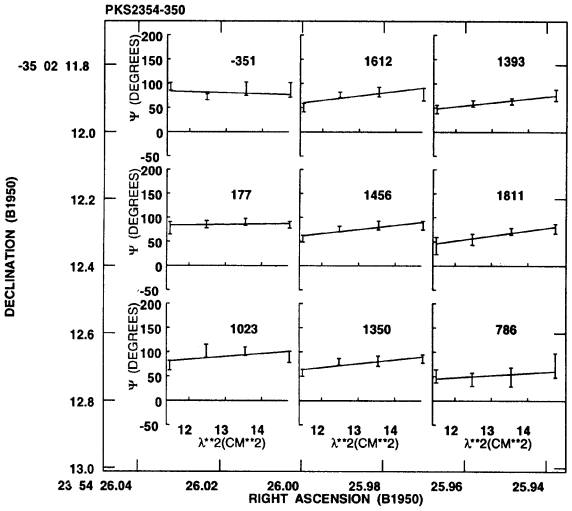

FIG. 14. Sample fits to the RM in the northwest lobe of PKS 2354−350. Error bars are drawn only if they would exceed the size of the plotted points.

The RMs throughout much of PKS 2354−350 are within the range of −300 to +300 radians m^{-2} (see Fig. 13), and are similar to the typical error in our estimation of the RM. There are three locations, however, of anomalously high RM. One small patch in the northwest lobe exhibits a RM of -2700 ± 500 radians m^{-2}, another somewhat larger region (a few beamwidths in size) just northwest of the radio core exhibits RMs of $\sim1500\pm400$ radians m^{-2} (see Fig. 14), as does another small region in the southwest lobe. This last region is adjacent to the region of very low fractional polarization. To produce a RM of 1500 radians m^{-2}, with a density distribution as observed by Schwartz *et al.* (1991) over a path length of 200 kpc requires a cluster magnetic field of >2.7 μG. This value is significantly larger than was found for the PKS 1508−059 cluster due to the much lower central density (0.008 cm^{-3}) of the hot gas surrounding PKS 2354−350. More sensitive, higher resolution observations are needed to better constrain the density of the hot gas in the central regions of the A4059 cluster.

The projected magnetic field direction in the radio source, corrected for RM, is shown in Fig. 15.

5. DISCUSSION

Examination of a flux-limited, all-sky x-ray sample of galaxies put forth by Edge *et al.* (1992) reveals that clusters with nonzero mass flow rates and embedded radio sources stronger than 100 mJy at 5000 MHz frequently display significant RMs. Of the 14 clusters in the sample that meet these criteria, 8 display an excess of 800 radians m^{-2}, two have RMs between 100 and 800 radians m^{-2}, one could not be measured (PKS 0745−191, see Sec. *4.5*), and three have not yet been measured. Cooling flow rates, x-ray luminosities (from 2–10 keV), RMs, and other relevant parameters

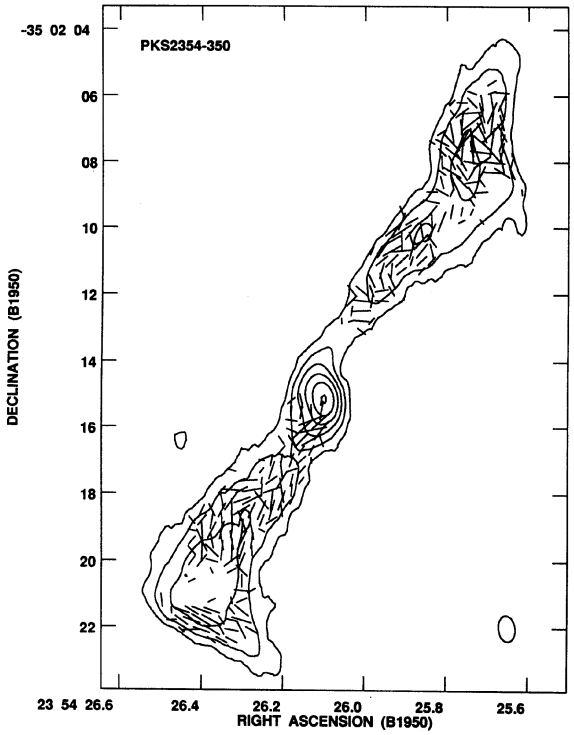

FIG. 15. The projected magnetic field direction, corrected for RM, in PKS 2354−350. A vector length of 1″ corresponds to a polarized intensity of 0.2 mJy $beam^{-1}$. Contours are taken from the 8350 MHz total intensity image and are the same as in Fig. 13.

TABLE 5. Radio sources in cooling flow clusters.

Cluster	Radio Source	z	$\dot{M}^a$ ($M_\odot$ yr^{-1})	log L_X (erg s^{-1})	Gal.^{b} Type	S_{5000} (Jy)	log P_{5000} (W Hz^{-1})	Size^c (kpc)	RM(1+z)^2 (rad m^{-2})	Ref.
Cygnus A	3C405	0.057	187	44.8	E	364	27.7	180	3000	1
Virgo A	3C274.0	18 Mpc	10	43.1	E	76	24.4	58	2000	2
Cen A	1322-42	3.5 Mpc	18	43.8	S0	63	23.0	500	-450	3
A426	3C84	0.0183	183	45.0	pec	50	25.9	640	N/A	4
Hydra A	3C218	0.0522	315	44.5	cD	14	26.3	670	-12000	5
A2052	3C317	0.0348	90	44.1	cD	1.0	24.7	39	-800	6
A2199	3C338	0.031	150	44.5	cD	0.48	24.3	67	2000	6
A119	0053-015	0.044	23	44.4	E	0.40	24.5	350	N/A	7
	0053-016	0.044	23	44.4	E	0.29	24.4	300	N/A	7
0745-191	0745-191	0.1028	702	45.4	cD	0.39	25.3	25	-^{d}	8
A2597	2322-123	0.0824	480	44.8	cD	0.33	25.0	10	N/A	9
A1795	4C26.42	0.062	478	44.9	cD	0.26	24.6	15	3000	6
3C129	0445+449	0.0208	61	44.3	E	0.25	23.7	500	-135^e	10
A4059	2354-350	0.0478	124	44.3	cD	0.11	24.0	70	-1500	8
A2029	1508+059	0.0767	402	45.3	cD	0.10	24.4	80	-8000	8

[a] The mass flow rate for a critical cooling time of 2×10^7 from Edge, Stewart & Fabian (1992).
[b] Galaxy type (E:elliptical; S0: lenticular; pec: peculiar, or cD: central dominant elliptical)
[c] The largest angular size of the radio source in kpc.
[d] No RM could be determined due to a lack of polarized emission (see Sec. 4.5).
[e] Downes (1984) reports that the RM values determined for 3C129 may suffer from $n\pi$ ambiguities.
References - (1) Dreher *et al.* 1987; (2) Owen *et al.* 1990; (3) Clarke, Burns & Norman 1992; (4) Burns *et al.* 1992; (5) Taylor & Perley 1993; (6) Ge 1991; (7) O'Dea & Owen 1985; (8) this work; (9) Ball, Burns & Loken 1993; (10) Downes 1984.

for these 14 galaxies are listed in Table 5. The RM value given is chosen from the region of largest RM which is coherent across a beamwidth or more with good polarized signal to noise. We have also plotted in Fig. 16 the RM as a function of cooling rate, $\dot{M}$. These results strongly suggest a correlation between the cooling rate and rotation measure. Even more striking is the fact that *all* of the known high RM sources (RM>700 radians m^{-2}; see Table 1 in Taylor *et al.* 1992) at low redshifts (z<0.4) are included in this x-ray selected sample. The high RM radio galaxy 3C 295 (Perley & Taylor 1991) at a redshift of 0.461 is also associated with a luminous x-ray cooling flow (Henry & Henriksen 1986),

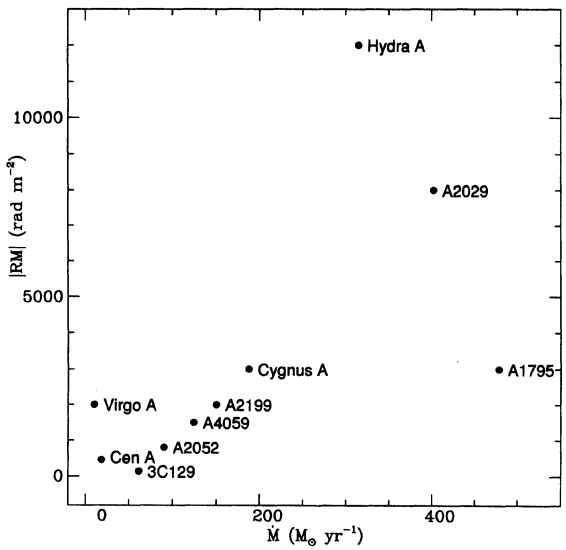

FIG. 16. The maximum absolute RM plotted as a function of $\dot{M}$ for the ten clusters in Table 5 with known RMs.

but the x-ray data for the remaining seven high RM, high z, sources are not good enough to distinguish between extended thermal emission and that from an active nuclear source. Beyond redshifts of ~0.4, low power radio sources like PKS 1508+059, and PKS 2354−350 are much too weak to allow for a determination of their RM. Most (6/8) of the high RM sources found at redshifts greater than 0.4 are CSS (compact steep spectrum) sources which have large radio powers and small sizes. The compact nature of the CSS sources, their frequently high RMs, and the frequent presence of a low frequency turnover in their spectra, possibly the result of free–free absorption, may indicate that these sources are also located in a dense environment (Taylor *et al.* 1992).

In addition to producing the high RMs, the dense cluster gas also appears to directly affect the embedded radio sources. The source with the largest inferred cooling flow rate, PKS 0745−191, has an amorphous shape, perhaps because the collimation of the usual bipolar flow has been disrupted by the dense ICM. Similar arguments have been suggested by Zhao *et al.* (1993) to explain another amorphous radio source, 3C317, embedded in an x-ray cooling flow. The notably steep spectra observed for PKS 0745−191, PKS 1508+059, and PKS 2354−350 (see Sec. *4.2*) argue in favor of these sources being confined by the ICM. Baum & O'Dea (1991) suggest that in radio sources that are not confined by an ICM, the old population of relativistic electrons undergo adiabatic losses, so that their synchrotron emissivity decreases and they do not contribute as strongly to the radio spectrum. In confined sources, this is not the case, so that these electrons produce a steeper spectrum. Roland *et al.* (1985) also suggest that sources of spectral index steeper than −1.3 are best understood if they are assumed to be confined by the intergalactic medium.

The observed change from negative to positive RM across the core of PKS 1508+059 strongly suggests a large scale

organization of the magnetic field. This phenomenon has been observed in Hydra A (Taylor & Perley 1993) and A1795 (Ge & Owen 1993). The scale of the organization of this field is roughly the size scale of the galaxy, ~100 kpc. Generating such large scale cluster magnetic fields will be a challenge for theorists.

6. CONCLUSIONS

Sensitive, high resolution images are presented for three radio sources embedded in x-ray cooling flow clusters. While PKS 0745−191 has been found to be unpolarized to less than <1%, absolute RMs as large as 2700 and 8000 radians m^{-2} are reported for PKS 2354−350 and PKS 1508 +059, respectively. These three sources, and all of the high RM sources with $z<0.4$, are included in the flux limited sample of Edge *et al.* (1992). For those cooling flow clusters with an embedded radio source, 57% (8/14), are found to have absolute RMs in excess of 800 radians m^{-2} indicating that the high RMs are related to the presence of dense cluster gas. Furthermore, a direct correlation is found between the RM and the cooling flow rate. We derive a minimum estimate of the cluster magnetic field strength of ~0.2 and ~2.7 μG in A2029 and A4059, respectively.

In addition to generating the observed cluster magnetic fields, the dense ICM in the three cooling flow clusters studied also interacts with the radio source. Thermal pressures derived from the x-ray observations meet or exceed minimum energy pressures in the radio sources. Confinement of the radio sources leads to much steeper than average radio spectra, and may disrupt the collimated flow in PKS 0745 −191. A direct comparison of high resolution x-ray and radio images for PKS 1508+059 has shown that the radio source flows out along pressure minima.

In a future paper we will present the VLA observations for the three sources that lack good radio polarimetry, and a statistical analysis of the radio sources embedded in cooling flow clusters.

The authors thank Craig Sarazin and Chris O'Dea for useful discussions and Craig Sarazin again for a *ROSAT* x-ray image of A2029. The authors also thank Tony Readhead for helpful comments on an earlier draft of the manuscript. This research has made use of the NASA/IPAC Extragalactic Database (NED) which is operated by the Jet Propulsion Laboratory, Caltech, under contract with NASA. G.B.T. and J.P.G. acknowledge support for this research from NSF under Grants Nos. AST-9117100 and AST-912282, respectively.

REFERENCES

Andernach, H., Tie Han, Sievers, A., Reuter, H.-P., Junkes, N., & Wielebinski, R. 1988, A&AS, 73, 265
Arnaud, K. A., Johnstone, R. M., Fabian, A. C., Crawford, C. S., Nulsen, P. E. J., Shafer, R. A., & Mushotzky, R. F. 1987, MNRAS, 227, 241
Baars, J. W. M., Genzel, R., Pauliny-Toth, I. I. K., & Witzel, A. 1977, A&A, 61, 99
Ball, R., Burns, J. O., & Loken, C. 1993, AJ, 105, 53
Baum, S. A., & O'Dea, C. P. 1991, MNRAS, 250, 737
Bautz, L. P., & Morgan, W. W. 1970, ApJ, 162, L149
Böhringer, H., Voges, W., Fabian, A. C., Edge, A. C., & Neumann, D. M. 1993, MNRAS, 264, L25
Burns, J. O. 1990, AJ, 99, 14
Burns, J. O., Sulkanen, M. E., Gisler, G. R., & Perley, R. A. 1992, ApJ, 388, L49
Carter, D., Inglis, I., Ellis, R. S., Efstathiou, G., & Godwin, J. G. 1985, MNRAS, 212, 471
Clarke, D. A., Burns, J. O., & Norman, M. L. 1992, ApJ, 395, 444
Conway, J. E. 1991, in Radio Interferometry: Theory, Techniques and Applications, edited by T. J. Cornwall and R. A. Perley (PASP, San Francisco), p. 171
Daly, R. A., & Loeb, A. 1990, ApJ, 364, 451
DeYoung, D. S. 1992, ApJ, 386, 464
Downes, S. 1984, MNRAS, 211, 215
Dreher, J. W., Carilli, C. L., & Perley, R. A. 1987, ApJ, 316, 611
Edge, A. C., Stewart, G. C., & Fabian, A. C. 1992, MNRAS, 258, 177
Eilek, J. A. 1993, ApJ (submitted)
Ekers, R. D., *et al.* 1989, MNRAS, 236, 737
Fabian, A. C., Nulsen, P. E. J., & Canizares, C. R. 1991, A&A, 2, 191
Ge, J. P. 1991, Ph.D. thesis, New Mexico Institute of Mining and Technology
Ge, J. P., & Owen, F. N. 1993, AJ, 105, 778
Goldman, I., & Rephaeli, Y., 1991, ApJ, 380, 344
Gull, S. F., & Northover, K. J. E. 1973, Nature, 244, 80
Heckman, T. M., Baum, S. A., van Breugel, W. J. M., & McCarthy, P. 1989, ApJ, 338, 48
Henry, J. P., & Henriksen, M. J. 1986, ApJ, 301, 689
Laing, R. A. 1980, MNRAS, 193, 439
Mackie, G., Visvanathan, N., & Carter, D. 1990, ApJS, 73, 637
Myers, S. T., & Spangler, S. R. 1985, ApJ, 291, 52
Norman, M. L., Burns, J. O., & Sulkanen, M. E. 1988, Nature, 355, 146
O'Dea, C. P., & Owen, F. N. 1985, AJ, 90, 927
Owen, F. N., Eilek, J. A., & Keel, W. C. 1990, ApJ 362, 449
Owen, F. N., White, R. A., & Burns, J. O. 1992, ApJS, 80, 501
Perley, R. A., Willis, A. G., & Scott, J. S. 1979, Nature, 281, 437
Perley, R. A., & Taylor, G. B. 1991, AJ 101, 1623
Pudritz, R. E., & Silk, J. 1989, ApJ, 342, 650
Roland, J., Hanisch, R. J., Veron, P., & Fomalont, E. 1985, A&A, 148, 323
Ruzmaikan, A. A., Sokoloff, D. D., & Shukurov, A. 1989, MNRAS, 241, 1
Sarazin, C. L. 1986, Rev. Mod. Phys. 58, 1
Sarazin, C. L., O'Connell, R. W., & McNamara, B. R. 1992, ApJ, 389, L59 (SOM)
Scheuer, P. A. G., & Williams, P. J. S. 1968, ARA&A, 6, 321
Schwartz, D. A., Bradt, H. V., Remillard, R. A., & Tuohy, I. R. 1991, ApJ, 376, 424
Soker, N., & Sarazin, C. L. 1988, ApJ, 327, 66
Sumi, D. M., Norman, M. L., & Smarr, L. L. 1988, in Cooling Flows in Clusters and Galaxies, edited by A. C. Fabian (Kluwer, Dordrecht), p. 257
Taylor, G. B. 1991, Ph.D. thesis, University of California at Los Angeles
Taylor, G. B., Perley, R. A., Inoue, M., Kato, T., Tabara, H., & Aizu, K. 1990, ApJ, 360, 41
Taylor, G. B., Inoue, M., & Tabara, H. 1992, A&A, 264, 421
Taylor, G. B., & Perley, R. A. 1993, ApJ, 416, 554
Taylor, G. B., & Perley, R. A. 1994, ApJ, in preparation
Tribble, P. C. 1989, MNRAS 238, 1247
Uson, J. M., Boughn, S. P., & Kuhn, J. R. 1991, ApJ, 369, 46
Windhorst, R. A., Mathis, D., & Neuschaefer, L. 1990, in The Evolution of the Universe of Galaxies, edited by R. G. Kron, ASP Conference Series (Bookcrafters, Provo), p. 389
Zhao, J.-H., Sumi, D. M., Burns, J. O., & Duric, N. 1993, ApJ, 416, 51